

Nuwa: A Quantum Circuit Transpiler Based on a Finite-Horizon Heuristic for Placement and Routing

Shengru Ren,^{1,*} KaWai Chen,^{1,*} Navid Ghadermarzy,^{1,*}
Brandon Nguyen,¹ Yanhao Huang,¹ and Pooya Ronagh^{1,2,3,4,†}

¹*1QB Information Technologies (1QBit), Vancouver, BC, Canada*

²*Institute for Quantum Computing, University of Waterloo, Waterloo, ON, Canada*

³*Department of Physics & Astronomy, University of Waterloo, Waterloo, ON, Canada*

⁴*Perimeter Institute for Theoretical Physics, Waterloo, ON, Canada*

We introduce a novel transpiler for the placement and routing of quantum circuits on arbitrary target hardware architectures. We use finite-horizon, and optionally discounted, reward functions to heuristically find a suitable placement and routing policy. We employ a finite lookahead to refine the reward functions when breaking a tie between multiple policies. We benchmark our transpiler against multiple alternative solutions and on various test sets of quantum algorithms to demonstrate the benefits of our approach.

I. INTRODUCTION

Classical optimization plays an important role in the study and development of quantum computing software–hardware stacks. Various layers of compilers must be used to transform a quantum algorithm written in a quantum programming language [23] to form an executable algorithm on a quantum processor. Ideally, this process can be fully automated so that a quantum software developer can abstract her attention away from considerations of optimal commutations of quantum gates [18, 19], mitigating various sources of noise and errors on the executed instruction sets [29], and the specific architectures of backend quantum devices [24].

An optimization problem related to compiling for a specific architecture requires the construction of an efficient transformation of the quantum program into one executable on specific systems of physical or logical qubits with geometric locality constraints such as 2D or 3D nearest-neighbour connectivity or other limited sets of multi-qubit entangling gates. This compilation step is of interest for the near-term compilation of small- to moderate-sized quantum algorithms on noisy, intermediate-scale quantum (NISQ) systems that have between tens and thousands of qubits [35]. Moreover, similar compilation procedures are of interest for fault-tolerant quantum computation (FTQC) on the large-scale architectures anticipated for quantum computers, such as modular architectures comprising arrays of superconducting qubits [22] or quantum dots and donors [44], and modular trapped-ion architectures dependent on shuttling ions between different trapping zones [3].

The goal of the aforementioned optimization task is to compile an input quantum circuit, written as an abstract sequence of quantum gates, into another circuit comprising quantum gates physically available on the target quantum processor while incurring the least possi-

ble overhead. A compiler that performs this translation may instead be called a *transpiler*, especially when the circuit transformation is happening at the same level of software abstraction (e.g., when both the input quantum circuit and the compiled circuit are written in terms of the Clifford + T gates), as opposed to when the compilation is from a higher level of abstraction to a lower one. The transpiler may aim to reduce the total number of additional gates it introduces in order to minimize the number of erroneous operations performed. Alternatively, the transpiler may reduce the depth, or *makespan*, of the compiled circuit in order to reduce the overall runtime of the algorithm, assuming that simultaneous gates can be performed with a negligible amount of cross-talk. In this paper, we focus on the former optimization objective of reducing the total number of additional gates the transpiler introduces.

This optimization problem is often modelled as a *placement and routing* problem of finding a mapping of the abstract qubits to the physical qubits (placement), followed by iterations of performing entangling gates between qubits that are far apart by moving them closer to each other (routing), for example, via SWAP gates. The placement and routing problem has been extensively studied in the context of NISQ algorithms [2, 4, 6, 10, 16, 18, 21, 22, 25, 28–31, 33, 38–40, 45, 46, 48, 51, 52], as well as in the fault-tolerant compilation of quantum algorithms using concatenated error-correcting codes [26], lattice surgery–based fault-tolerant quantum computing (FTQC) [22, 32], and defect-based FTQC [20].

Additionally, the placement problem has been specifically studied in [9, 11, 12, 42]. Our focus in this paper is on developing techniques for routing, although we use them to choose good placements as well as in cases where multiple options are available. We should also distinguish the literature cited herein and our paper from the works [13, 43, 47, 49, 50], wherein architectural considerations are incorporated with compilers operating at the circuit synthesis level.

The problem and several of its variants are known

* These authors contributed equally to this work.

† Corresponding author: pooya.ronagh@1qbit.com

to be NP-hard [6, 40]. Therefore, several of the mentioned references rely on heuristic methods for finding a (sub-)optimal placement and routing policy. Some of the solutions relevant to our approach are those based on the observation that the placement and routing problem is an inherently temporal problem over the span of multiple decision epochs. This includes an exact, but exponentially expensive, dynamic programming solution introduced in [40], temporal planning and constraint programming [2, 45], integer programming [30], and methods that use reinforcement learning [16, 39]. On one hand, these approaches are superior to the greedy techniques that neglect the future impact of decisions made at earlier decision epochs. On the other hand, the global nature of the optimization problem solved hinders the scalability of the algorithm, especially in instances where the compilation procedure is expected to include computationally intensive subroutines such as the training of neural networks.

In this paper, we propose a middle-ground solution to the problem that captures both the efficiency of heuristic and greedy approaches, and the optimality of dynamic programming solutions in temporal decision making problems. This results in an algorithm that scales favourably in the SWAP gate overhead compared to other algorithms. As shown in Section IV and Appendix B, our algorithm achieves superior scaling compared to the state-of-the-art transpilers for general quantum circuits [4, 41]. We note that while [51] and [28] show improved results over those of [41] for small circuits, a scalable performance improvement is not evident from these papers. In addition, [21] and [46] customize the transpilation problem for 2-local Hamiltonian simulation circuits whereas our algorithm is not specific to the type of input quantum algorithm (see also Fig. 6 for the benchmarking results of our algorithm on different types of quantum circuits).

A. An Overview of Our Algorithm

Although our algorithm is a heuristic search method, it is inspired by techniques in approximate dynamic programming [34], as will be apparent from the terminology we use. We introduce two *reward functions*, the placement score Eq. (5) and edge score Eq. (6), that resemble the (possibly discounted) cumulative reward structures in dynamic programming and reinforcement learning. However, instead of performing costly exact or approximate dynamic programming recursions on them, we restrict their definitions to a finite *decision horizon* in which only a finite number of subsequent two-qubit gates are taken into account. We then use heuristic search to decide on the immediate actions to take, that is, the placement and routing of a subsequent *layer* of gates. The full placement and routing *policy* is formed by iterating over this process. The reward functions introduce two hyperparameters, namely, a *discount factor* and the deci-

sion horizon. These hyperparameters are used to tune the significance of future gates within the decision horizon on the values of the reward functions and, consequently, on the routing policy.

Calculating the finite-horizon reward functions frequently results in a tie across multiple routing options. This result is more prominent in the case of more-structured quantum circuits, which constitute most of the practical input circuits of the transpiler. Our algorithm uses a tie-breaking subroutine (Section III B 1) to refine the routing decisions. We use a hyperparameter called the *lookahead depth* to determine how many decisions to take into account (i.e., the number of SWAP gates we intend to insert) in order to refine the evaluation of our immediate actions when a tie occurs between the reward function values.

Our transpiler is agnostic with respect to hardware architectures; it is capable of receiving a representation of the connectivity of any target architecture as an input. Moreover, the hyperparameters decision horizon, discount factor, and lookahead depth allow our algorithm to adapt to the structure and recurrent patterns of the input quantum circuits and the classical computing budget available to it in order to provide a suitable (sub-)optimal placement and routing policy.

B. Related Literature

We provide a detailed description of our approach in Section III, and in Section IV we demonstrate the superior performance of our transpiler against other algorithms proposed in the recent literature that, to our knowledge, are representative of the state of the art. Having said that, our approach incorporates several ideas from these competitors, which in this section we summarize comparatively.

We use two distinct routines for placement and routing. Our algorithm first chooses a placement by generating a set of candidates and ranking them according to their placement scores (Section III A). In principle, any placement can be considered in this ranking, but in this paper we confine our routine to generating candidate placements using the approaches of [6] and [4]. [6] uses a linear path built from the connectivity between qubits to find the initial placement, and in [4] a matching-based method is used (see Section III A 2 and Section III A 1 for more-detailed descriptions of the two placement methods). Neither of these references provide or utilize a systematic metric for comparing multiple placements with each other, whereas our placement score incorporates the effect of future gates in the input circuit for the purpose of this comparison.

In contrast, [25] iterates between a forward and backward traversal of the sequence of two-qubit gates in order to generate a placement that takes future gates into account. This procedure is used to update the initial placement while routing the qubits in the forward and

backward passes using a heuristic. As such, [25] does not use separate stages for placement and routing; instead, the two tasks are intertwined. Iterating over this process becomes more expensive as the depth of the circuit grows and there is no guarantee that a greater number of iterations will produce better transpilations of the input circuit. On the other hand, [25] uses two sets of future gates (in either the forward or reverse passes), the gates to be processed immediately in the execution order and a subsequent set of future gates, to rank possible routing options. The idea of using future gates in a heuristic search to make better routing decisions is systematically incorporated in our work using the (discounted and cumulative) edge scores with a tunable hyperparameter that varies the impact of gates in future layers (see Section II and Section III B for the definitions of the concepts of layers and edge scores, respectively).

Unlike the strategy taken in [25], [4] presents the finding that a routing scheme chosen in a greedy fashion performs better overall in numerical benchmarking. In [6], the routing policy is also chosen greedily and based on the two-qubit gates to be processed immediately in the execution order. A distance vector is incorporated in this process. The SWAP gate is chosen from a set of candidates that reduces the greatest distance between pairs of qubits that are involved in two-qubit gates in line to be executed. The process is continued until either there is only one candidate left or a predefined limit has been reached. If this method fails, in [6] the same strategy is repeated on pairs of SWAP gates instead of individual ones, and if this also fails it resorts to brute force by routing maximally distant qubits involved in a two-qubit gate towards each other in order to escape this situation.

We also use a similar myopic strategy for routing (see the definition of immediate edge scores in Section III B). However, according to our findings, symmetries of the input circuit can frequently cause degenerate decisions in a myopic routing strategy. This is why in our tie-breaking subroutine (Section III B 1) we use the more general edge scores (with discounted contributions from gates in the further layers included) to choose the edge that leads to the minimum number of future SWAP gates needed within the decision horizon.

Finally, it is worth noting that [25] and [4] consider the trade-off between optimizing the number of inserted SWAP gates and the depth of the circuit (assuming independent gates can be executed concurrently). However, in this paper, we focus on optimizing the total number of additional gates, assuming the near-term and intermediate-scale scenarios in which the quantum state can to some extent be protected against decoherence (using techniques such as dynamic decoupling, error mitigation, and error correction). However, higher SWAP overhead and the cross-talk caused by performing multiple gates concurrently are both more detrimental to the performance of a quantum device.

II. THE PLACEMENT AND ROUTING PROBLEM

The problem of interest in this paper is as follows. Given an input quantum circuit, or *input circuit*, we wish to find a second circuit, or *compiled circuit*, that executes the quantum algorithm but uses the quantum gates available on a physical device, called the *target architecture*, or architecture for short. We assume that the input circuit is determined by a sequence

$$\sigma = (g_1, \dots, g_N) \quad (1)$$

of N single-qubit rotations and CNOT gates afflicting a set

$$Q = \{q_1, \dots, q_M\} \quad (2)$$

of M (logical) qubits. The target architecture of the physical device also allows it to perform similar gates, but CNOT gates are not available between all pairs of physical qubits. The goal of our algorithm is to generate a compiled circuit that can be executed on the target architecture by inserting a plurality of SWAP gates in the sequence. We note that every SWAP gate can be performed using three CNOT gates. As the addition of gates creates a deeper circuit, the compiled circuit is more prone to errors and takes a longer time to execute. Therefore, our compiler has to minimize the number of inserted SWAP gates, from here on called the *SWAP count*, N_S .

Figure 1(a) shows a representation of an input circuit. The target architecture to which we intend to compile our quantum algorithm is represented using an undirected graph called a *coupling graph*, $G = (V, E)$, with vertices V and edges E . Each physical qubit is represented as a vertex $v \in V$ and the two-qubit gates available between physical qubits are represented by the edges $\{u, v\} \in E$ between the vertices u and v . We do not consider direction for the edges in this paper; however, our algorithm can be adapted to the case of devices with a particular direction for two-qubit gates as in the case of [7]. Figure 1(b) shows the coupling graph of the IBM Q20 Tokyo chip as an example target architecture [17].

We construct a *layering* for the input circuit, which is

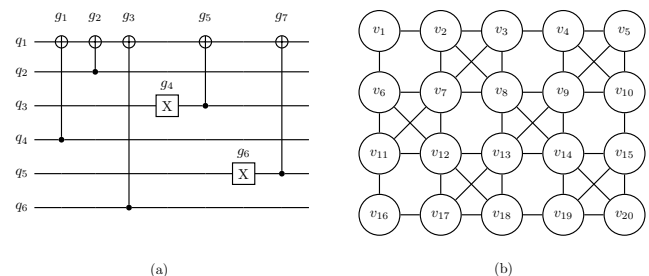


FIG. 1. (a) Example circuit with seven gates and six qubits. (b) Undirected coupling graph of the IBM Q20 Tokyo chip.

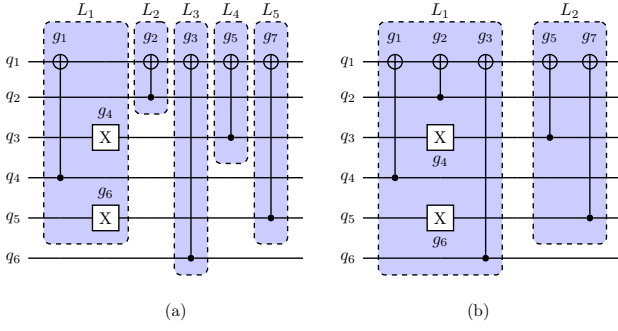


FIG. 2. Example circuit after gates are grouped into layers using (a) fine layering and (b) coarse layering. Each highlighted box represents a layer. Gates in a given highlighted box belong to the same layer.

a partition

$$L = \bigsqcup_{i=1}^{N_L} L_i \quad (3)$$

of the set of all gates in the input circuit σ into N_L layers. Each layer comprises a subset of the gates in σ . The layering is alternatively given by a function

$$\ell: \{g_1, \dots, g_N\} \rightarrow \mathbb{N}, \quad (4)$$

where $\ell(g_i)$ is the index of the layer to which gate g_i belongs. We perform this decomposition in two ways. In both cases, we assure the minimal number of layers are constructed. The construction also guarantees that the gates in the same layer can be executed in any order.

In the first decomposition, called *fine layering*, gates that share qubits are grouped into distinct layers. Figure 2(a) shows an example of fine layering. The single-qubit gates are moved to the earliest layer to which they can be moved. The single-qubit gates do not affect the placement and routing procedure explained in this paper.

In the second decomposition, called *coarse layering*, gates that mutually commute are allowed to be in the same layer. The commuting relations we use are the same ones used in [18], and are shown in Fig. 3. An example of coarse layering can be seen in Fig. 2(b). The motivation for using coarse layering is that all commuting gates

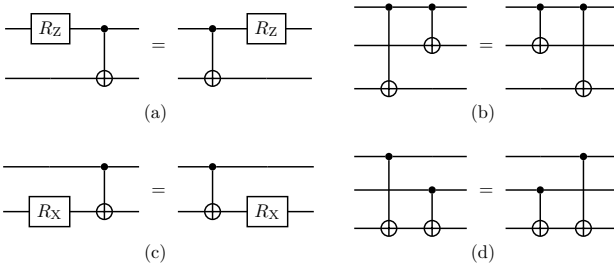


FIG. 3. (a) R_Z -control, (b) Control-control, (c) R_X -target, and (d) Target-target.

within the same layer can be executed in any order, thus reducing the potential SWAP count, N_S .

III. DESCRIPTION OF OUR ALGORITHM

Our algorithm consists of two main subroutines: placement and routing. We describe our method for finding a good placement in Section III A, and then present our routing subroutine in Section III B.

A. Placement

The first step of our algorithm is to assign each qubit in the circuit to a vertex. An injective mapping

$$p: Q \rightarrow V$$

of qubits involved in the input circuit σ to vertices of the coupling graph is called a *placement*. To a placement p we associate a *placement score*

$$\Sigma_{p,\ell}(\lambda, \delta) = \sum_{q \in Q} \sum_{g \in \sigma_{q,\lambda}} \delta^{\ell(g)-1} d_G(p(g_1), p(g_2)), \quad (5)$$

where λ is a positive integer called the *decision horizon*, or *horizon* for short. For each qubit in Q , the horizon represents the number of future gates in the circuit taken into account in order to evaluate the utility of a placement. For every qubit $q \in Q$, the set $\sigma_{q,\lambda} \subseteq \sigma$ is the subset of the first λ gates g in σ acting on q with a unique other qubit involved. Here, $g = (g_1, g_2)$ is a gate acting on qubits g_1 and g_2 , and d_G denotes the distance between vertices in the coupling graph G . The value $\delta \in [0, 1]$ is called the *discount factor*, and represents the significance of the contribution of later gates to the placement score. Discount factors closer to 0 aggressively suppress the contribution of gates in future layers, sorting them in chronological order, roughly speaking, whereas discount factors closer to 1 assign larger, yet exponentially decaying, weights on the distances between qubits involved in gates in future layers, allowing the future gates to make greater contributions. The best choice of discount factors depends on the structure of the input circuit. The hyperparameters decision horizon and discount factor appear also in the definition of edge scores in Section III B. We study the effect of these hyperparameters on the performance of our algorithm in Appendix A.

A good placement is one that can lead to a significant reduction in the final SWAP gate count. We present two heuristics for generating placements: *matching-based* and *linear* placement. We generate a number of placements using the two heuristics. We then compare the placements with each other using the placement score Eq. (5). Afterwards, we use the placement with the lowest placement score to route the circuits.

1. Matching-based placement

This method involves finding a maximal matching on the coupling graph, and constructing a placement that maps the gates of the first layer onto the edges of the matching. The idea of using a matching in the coupling graph was first introduced in [4].

We employ two methods for finding a matching. The first is a greedy approach, in which edges are added to the matching until no additional edges can be added. The second approach is to use Edmonds' blossom algorithm [8] to construct a maximum matching. In general, a maximum matching covers a larger number of target qubits. However, the blossom algorithm takes more computation time than the greedy matching and its effect is not significant for highly structured coupling graphs such as regular lattices. We refer the reader to Table I for a comparison of the performance of the greedy and blossom matching methods.

Using a matching in the coupling graph might not result in a complete placement. The remaining qubits without an assigned placement can be mapped to the remaining vertices at random. However, this may cause the qubits to be assigned to vertices that are far apart, especially when the number of vertices is much larger than the number of qubits. This would require us to introduce unnecessary SWAP gates in the compiled circuit in order to move the qubits closer to each other. To prevent this behaviour, we introduce another heuristic to keep the placed qubits closer to the more-connected regions in the architecture.

2. Linear placement

We construct maximal paths in the coupling graph using a greedy algorithm. This is done in two ways: the algorithm greedily favours either the high-degree or low-degree vertices. The latter method is used to account for architectures that have star-like subgraphs, for which starting from the highest-degree vertices might result in very short paths (see Fig. 4 for an example). For more-complex architectures, this greedy approach can be performed continually until a maximal linear forest has been found.

After the paths are constructed, the placement algorithm iterates through the vertices of any given longest path and moves the qubits to the earliest free vertices on the path.

As demonstrated in Section IV A, the two heuristics introduced above can be used as stand-alone methods or in combination. Optionally, a plurality of placements can be generated and compared according to their placement scores.

B. Routing

The placement provided in Section III A is used as input for our routing subroutine. Its pseudocode is shown in Algorithm 1. The goal of the algorithm is to identify a set of edges in the coupling graph along which SWAP gates will be inserted.

Algorithm 1: Routing Algorithm

Input: Input circuit σ , target architecture G , a layering $L = \sqcup L_i$, and a placement p
Output: Compiled circuit τ

```

1 Initialize the compiled circuit  $\tau$  as an empty sequence;
2 while  $\sigma$  is not empty do
3   Construct a sequence  $\rho$  of gates in  $L_1$  already
     executable on  $G$ ;
4   Update  $\tau$  by appending  $\rho$  to it;
5   Update  $\sigma$  by removing  $\rho$  from it;
6   Recompute the layering for  $\sigma$ ;
7   for every free qubit  $q$  in the input circuit do
8     Change the placement of  $q$  if a different
       placement improves the placement score;
9   end
10  if there are no executable gates in  $L_1$  then
11    Calculate the edge scores for edges incident to
      vertices involved in  $L_1$ ;
12    if the optimal edge score is degenerate then
13      Use subroutine presented in Section III B 1
        to break the tie;
14    else
15      Append a SWAP gate along the optimal
        edge to  $\tau$ ;
16    end
17  end
18 end

```

The routing algorithm receives an input circuit σ and iteratively constructs a compiled circuit τ . The algorithm begins by finding *executable* gates in the first layer, L_1 . Here, a gate in L_1 is called executable if the qubits involved in the layer are mapped by the placement function to adjacent vertices on the coupling graph. If we find executable gates, they are removed from L_1 and added to τ in the order they appear in σ .

We then revise the layering, which updates L_1 . At

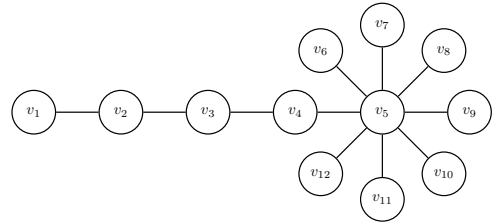


FIG. 4. Example architecture containing a star-like subgraph. Starting path construction from v_5 might result in a short path, whereas starting from v_1 will result in a longer path.

this point, if there are more vertices than qubits, some of the vertices will not be in the image of the placement function. We note that, if a qubit has not yet been used in any gate in τ , the qubit is free to be reassigned to an unoccupied vertex or exchange places with another unused qubit. We call such qubits *free qubits*.

After updating L_1 , for every free qubit found in the input circuit, we ascertain whether a different placement for the free qubit improves its placement score, in which case we update the placement of the qubit. If all qubits in σ have already been included in τ , as there are no free qubits, this heuristic step will not be executed.

If no executable gates are found, the algorithm finds a number of edges to insert SWAP gates along such that the qubits involved in non-executable gates are swapped to adjacent vertices, rendering them executable. Since SWAP gates can be inserted on any edge in the coupling graph, we need to determine which edge would be the best next choice.

An edge $e = \{q_1, q_2\} \in E$ in the coupling graph is a good choice if it results in fewer future SWAP gates according to our routing algorithm. We determine such an edge using its *edge score*, which we define as a summation

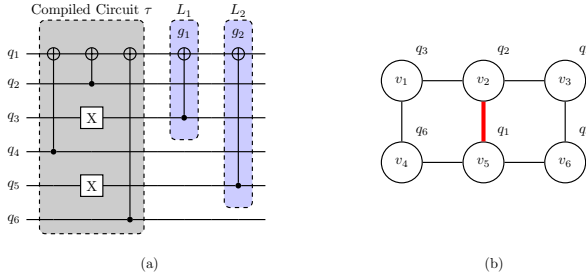


FIG. 5. (a) Example circuit with gates in τ already routed, gate g_1 in layer L_1 , and gate g_2 in layer L_2 . (b) Mapping of the circuit on a 2×3 grid. We first need to identify the gate(s) in L_1 , which is g_1 in this example. To perform an edge score calculation, we inspect edges (v_1, v_2) and (v_1, v_4) , which are incident to the vertex of q_3 , and edges (v_4, v_5) , (v_2, v_5) , and (v_5, v_6) , which are incident to the vertex of q_1 . Here, we show how to calculate the edge score for edge (v_2, v_5) , shown in red. We denote the edge by $e_{25} = (v_2, v_5)$. For qubit q_1 , the next not-yet-routed gate is gate g_1 , which is in layer L_1 , and the other qubit in g_1 is q_3 , which is mapped to vertex v_1 . Using Eq. (6), the immediate edge score is then calculated to be $\Omega_{p,\ell}(e_{25}) = d_G(v_1, v_5) - d_G(v_1, v_2) = 1$. Similarly, for the discounted score, the next not-yet-routed gate after g_1 is g_2 , which is in layer L_2 , and the other qubit in the gate is q_5 , which is mapped to vertex v_3 . The edge score that includes gates in both L_1 and L_2 is then calculated to be $\Omega_{p,\ell}(\lambda = |L_1| + |L_2|, \delta = 0.1, e_{25}) = (d_G(v_1, v_5) - d_G(v_1, v_2)) + 0.1(d_G(v_3, v_5) - d_G(v_2, v_3)) = 1.1$. As for the other vertex v_2 of e_{25} , given that it does not contain a qubit which corresponds to the gate in L_1 , no calculation is needed.

of two terms

$$\Omega_{p,\ell}(\lambda, \delta, e) = \sum_{i=1,2} \Omega_{p,\ell}(\lambda, \delta, e, q_i). \quad (6)$$

Here, each $\Omega_{p,\ell}(\lambda, \delta, e, q_i)$ is zero if the first gate (not necessarily e) involving q_i is not in L_1 , and otherwise

$$\Omega_{p,\ell}(\lambda, \delta, e, q_i) = \sum_{g \in \sigma_{q_i, \lambda}^r} \delta^{\ell(g)-1} \left[d_G(p(g_1), p(g_2)) - d_G(p_e(g_1), p_e(g_2)) \right]. \quad (7)$$

Here, $\sigma_{q_i, \lambda}^r \subseteq \sigma$ is the set of the first λ gates in σ that act on q_i and one other qubit. The current placement p and the new placement p_e are associated with the edge e by switching the placement of the qubits mapped to q_1 and q_2 , if any exist. That is, $p_e(p^{-1}(q_1)) = q_2$ if q_1 is in the image of p , and, similarly, $p_e(p^{-1}(q_2)) = q_1$ if q_2 is in the image of p .

Unlike in the definition of $\sigma_{q, \lambda}$ in Section III A, we allow the repetition of gates in the definition of $\sigma_{q, \lambda}^r$, as it is natural to expect that each gate between the same qubits should affect the edge score. We also empirically verify that not enforcing the condition $\Omega_{p,\ell}(\lambda, \delta, e, q_i) = 0$ when the first gate involving q_i is not in L_1 results in worse performance for our algorithm.

Figure 5 provides an example of the edge score calculation. Here, λ represents the decision horizon and δ represents the discount factor. The extreme case of $\delta = 0$ is of particular interest, as it corresponds to the “myopic” decision horizon in which only the gates in the first layer are taken into account. The edge scores

$$\Omega_{p,\ell}(e) := \Omega_{p,\ell}(\lambda \geq |L_1|, \delta = 0, e)$$

are called *immediate* edge scores.

We use the immediate edge scores to heuristically find a convenient edge along which to insert a SWAP gate. It is sufficient to calculate the edge scores only for the edges that are incident to the vertices corresponding to the gates in L_1 . This is because inserting SWAP gates along edges that are not incident to qubits in L_1 has no impact on L_1 . We insert a SWAP gate along the edge with the maximum immediate edge score. If multiple edges are found to have the maximum edge score, we invoke a tie-breaking heuristic, which we explain in Section III B 1.

The routing algorithm iterates over the above procedure until there are no gates left in L_1 , at which point all gates have been routed and the algorithm terminates.

1. Tie-breaking subroutine

In many cases, multiple edges are found to have the maximum edge score. We call such edges *degenerate*. To break a tie between degenerate edges, the algorithm temporarily inserts a SWAP gate for each such edge. It then continues the routing procedure, using an edge score

with a decision horizon $\lambda > |L_1|$, until it generates a given number $D > 0$ of additional SWAP gates, or it terminates when the entire input circuit is compiled. The hyperparameter D is called the *lookahead depth*. For each degenerate edge, the goal of this multi-step lookahead is to inspect the future state of the placement score after the insertion of D SWAP gates within the decision horizon. We note that, compared to λ , D has to be sufficiently small for this D -step lookahead to remain within the decision horizon.

If, after the addition of D SWAP gates, the entire input circuit has not been routed, the placement score of the resulting placement is stored as a *tie-breaking score* for the degenerate edges.

However, if the entire input circuit has been routed with $D' \leq D$ additional SWAP gates, then the tie-breaking score of the degenerate edge is defined as $D' - D$. The tie-breaking procedure then selects the edge with the smallest tie-breaking score. If a degenerate case still occurs for the tie-breaking scores, then one of the degenerate edges is selected at random.

2. Complexity analysis

The time complexity of the routing procedure depends on the size of the input circuit, the number of steps required to calculate the insertion of a SWAP gate, and the number of tie-breaking subroutine calculations. To estimate the upper bound, we assume the worst case in our analysis. In this case, all qubits are involved in each step of the calculation. The routing procedure starts by performing an update on the layering, which has a complexity of $O(\lambda N)$, where N is the number of qubits. The computation of the immediate edge score has a complexity of $O(N)$. Assuming all edge scores are degenerate, we call the tie-breaking subroutine for all candidate edges. The subroutine's complexity depends on the lookahead depth D . For each of the candidate edges, we need to insert at most D SWAP gates. This leads to a time complexity of $O(DN)$. In total, the time complexity for routing a single gate is $O(\lambda N) + O(N) + O(DN)$. Using N_G to denote the total number of gates, the time complexity of our routing procedure is $O(N_G \cdot (\lambda + D)N)$.

IV. NUMERICAL RESULTS

In this section, we present our results and compare them with those of other placement and routing algorithms. To the best of our knowledge, SABRE [25] is a commonly used quantum compiler for benchmarking, `arct` [4] scales well, and runs fast for large circuits, and `tket` [41] is the state-of-the-art library for general quantum circuits.

In Section IV A, we discuss the effects of different combinations of the placement schemes, introduced in Section III A, on the SWAP count. As part of an ablation

study, we benchmark the performance of our algorithm both with and without the application of the commutation rules presented in Fig. 3. Then, in Section IV B, we use a set of hyperparameters that provides a good balance between performance and runtime, and the best placement scheme found to compare our algorithm against the above-mentioned alternatives. We perform a hyperparameter study and find that while certain choices of hyperparameters are evidently inadequate (e.g., the discount factors $\delta = 0$ or 1), small circuits are not very sensitive to the values of the hyperparameters. The results of the study can be found in Appendix A.

A. Placement Heuristics

In our experiments, we benchmark three placement heuristics: (1) linear placement as a stand-alone placement heuristic; (2) the combination of matching-based placement and linear placement; and (3) a random mixture of the two methods to generate a plurality of placements, followed by performing a number of random SWAP gates before calculating the score of each placement. Methods (1) and (2) each generate a single placement, but method (3) generates multiple placements that are then compared to each other according to their placement scores, with the placement that has the best score being selected. We choose the hyperparameters $\delta = 0.1$, $D = 7$, and $\lambda = 40$ in our benchmarking, performing benchmarks on the test set of circuits provided in [25]. We select the hyperparameters here with the aim to strike a balance between performance and runtime for the circuits tested. We report our results in Table I.

As shown in Table I, method (1) performs best for Ising model circuits, independent of whether we apply commutation rules. This is expected, as the two-qubit gates in the circuits representing one-dimensional Ising models are CNOT gates that are applied to successive qubits. Given the linear structure of Ising model circuits, they are not representative of general benchmarking circuits; therefore, we exclude them from our discussion and the results in Table II.

We observe from Table I that method (3) produces the greatest number of best results for smaller circuits (i.e., circuits with fewer than 100 gates) among the benchmark tests we run, both with and without the application of commutation rules. However, for larger circuits (i.e., those having more than 400 gates), method (2B) produces the greatest number of best results, both with and without applying commutation, by taking advantage of the matching algorithms and randomness involved in producing the rest of the placements.

In Table II, we use the best results as a baseline. We calculate the average percentage increase in the SWAP count for each method, as compared to the baseline. On average, method (3) outperforms the other methods, and the use of commutation rules improves the performance of the transpiler. As a result, we use method (3) and

Circuit	No. of Qubits	No. of Gates	Avg. SWAP Count – Without Commutation				Avg. SWAP Count – With Commutation			
			(1)	(2A)	(2B)	(3)	(1)	(2A)	(2B)	(3)
4mod5-v1_22	5	21	3	3.33	2.33	2.33	2*	3	2.33	2*
mod5mils_65	5	35	4	4	4.67	2.33*	2.67	3	4.33	2.33*
alu-v0_27	5	36	3.33	5.67	6	3.33	2*	3.33	5.33	3.33
decod24-v2_43	4	52	5.67	5.67	5.67	3.33*	9.33	7.33	6	3.33*
4gt13_92	5	66	8.67	7	7.67	5.67	9.67	4.67	4.67	4*
ising_model_10	10	480	0*	7.33	9.67	5	0*	5.67	8	5
ising_model_13	13	633	0*	12	11	6.33	0*	10.67	11.67	6.67
ising_model_16	16	786	1	10.33	14	7.33	0*	14.67	14.33	6.33
rd84_142	15	343	49.33	59.67	52.67	43.33	39.67*	47	47.67	44.33
adr4_197	13	3439	325.67	302	277.33	318	293.67	263.67	248.33*	248.67
radd_250	13	3213	294.33	307	311	288.33	227.33*	257.33	245	258
z4_268	11	3073	277.67	260.67	253.33	270	210.33*	243.67	237.33	225.33
sym6_145	7	3888	324.67	314	220	282.67	231	264.67	201*	205.67
misex1_241	15	4813	345.33	339.67	351.33	311.33	282	275.33	326.33	268.67*
rd73_252	10	5321	430.67	480.33	486.33	412	375.33*	416	402	396.67
cycle10_2_110	12	6050	567.67	539.33	479.33	559	489.67	421.67*	468.67	456.33
square_root_7	15	7630	558	416*	563.33	523	431	519	501	420.33
sqn_258	10	10223	937.67	838	919	776	697.67	690.67*	747	693.33
rd84_253	12	13658	1332.67	1202.33	1272	1170.33	1043.33	1011.67	1067.67	1010*
co14_215	15	17936	1861.67	1682.33	1841	1850.67	1665.33	1630.67	1438*	1639.67
sym9_193	10	34881	3305	3272	3089.33	3249.33	2878.67	2782.67	2453*	2696.67
9symml_195	11	34881	3113.33	2945	3153	3034	2459	2674	2147.33*	2817
Number of Lowest SWAP Counts			2	1	0	2	9	2	5	6

TABLE I. SWAP counts with different placement methods performed on the test quantum circuits in [25]. Method (1): linear placement, method (2A): matching-based placement with greedy matching, method (2B): matching-based placement with blossom matching, and method (3): multiple placements. The lowest SWAP count for each circuit is shown in bold text and with an astrisk.

	(1)	(2A)	(2B)	(3)
Without Commutation	44.4%	45.5%	45.2%	24.9%
With Commutation	23.5%	24.1%	25.3%	9.1%

TABLE II. Average relative increase in the SWAP counts for each placement method shown in Table I. The relative increase percentages are with respect to the baseline, defined as the lowest SWAP count observed between all four methods. Method (1): linear placement, method (2A): matching-based placement with greedy matching, method (2B): matching-based placement with blossom matching, and method (3): multiple placements.

apply commutation rules for the following benchmark, in which we compare our algorithm’s performance against that of other algorithms.

B. Comparison with Other Algorithms

We first compare the results obtained from our transpiler, called Nuwa, with those produced by `arct` in [4] and `tket` in [41]. Several families of practically important quantum circuits have been contributed by [4, 37] for benchmarking purposes. We benchmark the three algorithms on these families, namely, quantum circuits per-

taining to quantum signal processing (QSP) [27], quantum Fourier transformation (QFT), and the product formula expansion of exponentials of local Hamiltonians, which is of interest in Hamiltonian simulation applications [5]. We also benchmark the three algorithms on randomly generated circuits. Note that the initial placements for the four algorithms are not identical.

The results of our comparison are shown in Fig. 6. On average, Nuwa uses 9.0% fewer SWAP gates than `tket` and 51.8% fewer SWAP gates than `arct` for QSP circuits. For QFT circuits, the average improvement is 22.4% and 52.6%, respectively. For product formula circuits, Nuwa uses 13.1% more SWAP gates than `tket` but 83.1% fewer than `arct`. For random circuits, the average improvement is 15.7% and 45.1%, respectively.

We next compare Nuwa’s results with those of Qiskit implementation [15] of SABRE. We use the same circuits as used in [25]. Results produced by `tket` are also included, and are shown in Table III. We note that we were not able to include SABRE in the study whose results are shown in Fig. 6 on test instances of [37], as the Qiskit implementation of SABRE requires the number of vertices of the coupling graph to be the same as the number of qubits in the input quantum circuit.

Nuwa outperforms other algorithms by a significant margin, both with and without applying commutation

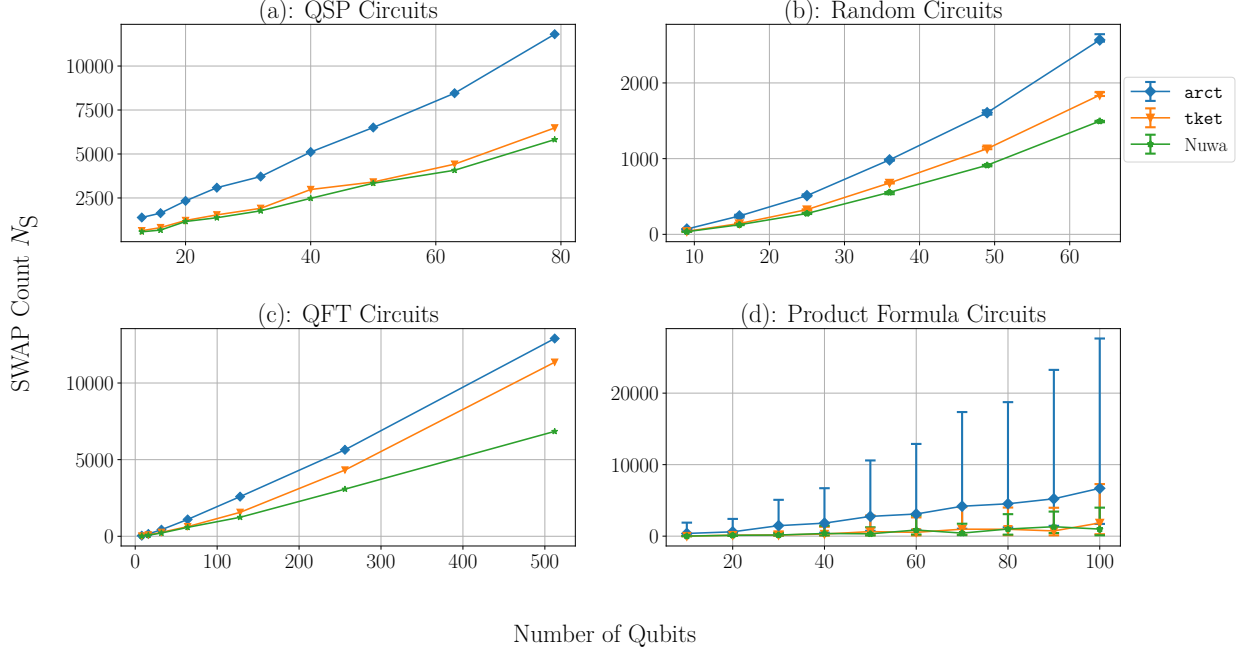


FIG. 6. (a) SWAP counts of the QSP circuits. (b) Average SWAP counts of randomly generated circuits. (c) SWAP counts of QFT circuits. (d) Average SWAP counts of the product formula circuits. For (b) and (d), we use the median and interquartile range for each average data point.

Circuit	No. of Qubits	No. of Gates	tket	SABRE	arct	Nuwa	
						Without Commutation	With Commutation
4mod5-v1.22	5	21	4	7	6	2.33	2*
mod5mils.65	5	35	3	17	7	2.33	2.33*
alu-v0.27	5	36	3	12	11	3.33	3.33*
decod24-v2.43	4	52	9	20	13	3.33	3.33*
4gt13.92	5	66	9	19	19	5.67	4*
ising_model.10	10	480	9	65	15	5	5*
ising_model.13	13	633	9	86	29	6.33*	6.67
ising_model.16	16	786	16	107	36	7.33	6.33*
rd84.142	15	343	37*	78	84	43.33	44.33
adr4.197	13	3439	440	670	837	318	248.67*
radd.250	13	3213	468	684	828	288.33	258*
z4.268	11	3073	369	713	743	270	225.33*
sym6.145	7	3888	332	897	792	282.67	205.67*
misex1.241	15	4813	662	1046	1132	311.33	268.67*
rd73.252	10	5321	716	1125	1208	412	396.67*
cycle10.2.110	12	6050	915	1178	1485	559	456.33*
square_root.7	15	7630	1007	1240	1526	523	420.33*
sqn.258	10	10223	1100	2435	2300	776	693.33*
rd84.253	12	13658	2013	2784	3060	1170.33	1010*
co14.215	15	17936	2727	3235	4860	1850.67	1639.67*
sym9.193	10	34881	5232	6211	7838	3249.33	2696.67*
9symml.195	11	34881	5232	6234	7838	3034	2817*
Number of Lowest SWAP Counts			1	0	0	1	20

TABLE III. SWAP counts for the four routing algorithms. The lowest SWAP count for each circuit is shown in bold text and with an astrisk. All tests have been performed on the IBM Q20 Tokyo coupling graph, represented in Fig. 1(b).

rules, except for the circuit `rd84_142`. Without applying commutation rules, Nuwa uses approximately 34% fewer SWAP gates than `tket` on average, and 66% fewer than SABRE. With commutation rules applied, the average improvement percentages are 40% and 71%, respectively.

Finally, we note that the benchmarking instances in [25] are extended to a larger set of input circuits in [53]. We refer the reader to Appendix B for the results of this extended benchmarking performed using two target architectures.

V. CONCLUSION

The development of quantum circuit compilers and transpilers requires exploration and incorporation of classical optimization and operations research techniques. Not only are these compilers and transpilers expected to fulfill critical roles in future quantum computing software stacks, but to serve as important research tools for the production of architecture-aware resource estimations for quantum algorithms. Transpilers could, in turn, be used to find improved architectures for quantum devices, and to provide more-accurate estimates of the number and fidelity of gates required for practical applications [1, 14, 36].

In this paper, we have introduced a novel transpiler for the placement and routing of qubits on a target architecture. Our transpiler uses a finite decision horizon to evaluate two (possibly discounted) rewards: the placement and edge score functions. It also incorporates a fi-

nite lookahead tie-breaking subroutine. We have benchmarked our transpiler against multiple alternative solutions and on various test sets. We showed that our algorithm performs significantly better compared to other algorithms when the circuits contain a large number of gates.

Quantum resources are much more scarce than classical computing resources, which justifies transpilers spending substantial classical computing resources in the optimization of placement and routing policies. It is, however, important to have scalable solutions that can be employed on larger quantum circuits or adapted to fault-tolerant circuit compilation for much larger quantum algorithms. In addition, it is important for the transpiler to be flexible with respect to target architectures. This flexibility allows us to use transpilers as research tools for quantitative analysis of the overhead of compiling quantum algorithms on various target architectures. Our transpiler provides these critical advantages while improving the state of the art.

ACKNOWLEDGMENTS

This project was funded by 1QBit. P. R. additionally acknowledges the financial support of Mike and Ophelia Lazaridis, and Innovation, Science and Economic Development Canada. All authors thank our editor, Marko Bucyk, for his careful review and editing of the manuscript.

-
- [1] Ryan Babbush, Jarrod R McClean, Michael Newman, Craig Gidney, Sergio Boixo, and Hartmut Neven. 2021. Focus beyond quadratic speedups for error-corrected quantum advantage. *PRX Quantum* 2, 1 (2021), 010103.
 - [2] Kyle Booth, Minh Do, J Beck, Eleanor Rieffel, Davide Venturelli, and Jeremy Frank. 2018. Comparing and integrating constraint programming and temporal planning for quantum circuit compilation. In *Proceedings of the International Conference on Automated Planning and Scheduling*, Vol. 28.
 - [3] Kenneth R Brown, Jungsang Kim, and Christopher Monroe. 2016. Co-designing a scalable quantum computer with trapped atomic ions. *npj Quantum Information* 2, 1 (2016), 1–10.
 - [4] Andrew M Childs, Eddie Schoute, and Cem M Unsal. 2019. Circuit transformations for quantum architectures. *arXiv preprint arXiv:1902.09102* (2019).
 - [5] Andrew M Childs, Yuan Su, Minh C Tran, Nathan Wiebe, and Shuchen Zhu. 2021. Theory of trotter error with commutator scaling. *Physical Review X* 11, 1 (2021), 011020.
 - [6] Alexander Cowtan, Silas Dilkes, Ross Duncan, Alexandre Krajenbrink, Will Simmons, and Seyon Sivarajah. 2019. On the qubit routing problem. *arXiv preprint arXiv:1902.08091* (2019).
 - [7] Gerhard W Dueck, Anirban Pathak, Md Mazder Rahman, Abhishek Shukla, and Anindita Banerjee. 2018. Optimization of Circuits for IBM’s five-qubit Quantum Computers. In *2018 21st Euromicro Conference on Digital System Design (DSD)*. IEEE, 680–684.
 - [8] Jack Edmonds. 1965. Paths, trees, and flowers. *Canadian Journal of mathematics* 17 (1965), 449–467.
 - [9] Hongxiang Fan, Ce Guo, and Wayne Luk. 2022. Optimizing quantum circuit placement via machine learning. In *Proceedings of the 59th ACM/IEEE Design Automation Conference*. 19–24.
 - [10] Azim Farghadan and Naser Mohammadzadeh. 2017. Quantum circuit physical design flow for 2D nearest-neighbor architectures. *International Journal of Circuit Theory and Applications* 45, 7 (2017), 989–1000.
 - [11] Blake Gerard and Martin Kong. 2021. Exploring Affine Abstractions for Qubit Mapping. In *2021 IEEE/ACM Second International Workshop on Quantum Computing Software (QCS)*. IEEE, 43–54.
 - [12] Blake Gerard and Martin Kong. 2021. String Abstractions for Qubit Mapping. *arXiv preprint arXiv:2111.03716* (2021).
 - [13] Vlad Gheorghiu, Jiaxin Huang, Sarah Meng Li, Michele Mosca, and Priyanka Mukhopadhyay. 2022. Reducing the CNOT count for Clifford+ T circuits on NISQ archi-

- tures. *IEEE Transactions on Computer-Aided Design of Integrated Circuits and Systems* (2022).
- [14] Craig Gidney and Martin Ekerå. 2021. How to factor 2048 bit RSA integers in 8 hours using 20 million noisy qubits. *Quantum* 5 (2021), 433.
 - [15] Abraham Héctor et al. 2019. Qiskit: An Open-source Framework for Quantum Computing. Retrieved from DOI: DOI: <https://doi.org/10.5281/zenodo.2562110> (2019).
 - [16] Steven Herbert and Akash Sengupta. 2018. Using reinforcement learning to find efficient qubit routing policies for deployment in near-term quantum computers. *arXiv preprint arXiv:1812.11619* (2018).
 - [17] Stefan Hillmich, Alwin Zulehner, and Robert Wille. 2021. Exploiting Quantum Teleportation in Quantum Circuit Mapping. In *2021 26th Asia and South Pacific Design Automation Conference (ASP-DAC)*. IEEE, 792–797.
 - [18] Toshinari Itoko, Rudy Raymond, Takashi Imamichi, and Atsushi Matsuo. 2020. Optimization of quantum circuit mapping using gate transformation and commutation. *Integration* 70 (2020), 43–50.
 - [19] Toshinari Itoko, Rudy Raymond, Takashi Imamichi, Atsushi Matsuo, and Andrew W Cross. 2019. Quantum circuit compilers using gate commutation rules. In *Proceedings of the 24th Asia and South Pacific Design Automation Conference*. 191–196.
 - [20] Ali Javadi-Abhari, Pranav Gokhale, Adam Holmes, Diana Franklin, Kenneth R Brown, Margaret Martonosi, and Frederic T Chong. 2017. Optimized surface code communication in superconducting quantum computers. In *Proceedings of the 50th Annual IEEE/ACM International Symposium on Microarchitecture*. 692–705.
 - [21] Lingling Lao and Dan E Browne. 2022. 2qan: A quantum compiler for 2-local qubit hamiltonian simulation algorithms. In *Proceedings of the 49th Annual International Symposium on Computer Architecture*. 351–365.
 - [22] Lingling Lao, Bas van Wee, Imran Ashraf, J van Someren, Nader Khammassi, Koen Bertels, and Carmen G Almudever. 2018. Mapping of lattice surgery-based quantum circuits on surface code architectures. *Quantum Science and Technology* 4, 1 (2018), 015005.
 - [23] Ryan LaRose. 2019. Overview and comparison of gate level quantum software platforms. *Quantum* 3 (2019), 130.
 - [24] Frank Leymann and Johanna Barzen. 2020. The bitter truth about gate-based quantum algorithms in the NISQ era. *Quantum Science and Technology* 5, 4 (2020), 044007.
 - [25] Gushu Li, Yufei Ding, and Yuan Xie. 2019. Tackling the qubit mapping problem for NISQ-era quantum devices. In *Proceedings of the Twenty-Fourth International Conference on Architectural Support for Programming Languages and Operating Systems*. 1001–1014.
 - [26] Chia-Chun Lin, Susmita Sur-Kolay, and Niraj K Jha. 2014. PAQCS: Physical design-aware fault-tolerant quantum circuit synthesis. *IEEE Transactions on Very Large Scale Integration (VLSI) Systems* 23, 7 (2014), 1221–1234.
 - [27] Guang Hao Low and Isaac L Chuang. 2017. Optimal Hamiltonian simulation by quantum signal processing. *Physical review letters* 118, 1 (2017), 010501.
 - [28] Abtin Molavi, Amanda Xu, Martin Diges, Lauren Pick, Swamit Tannu, and Aws Albarghouthi. 2022. Qubit Mapping and Routing via MaxSAT. In *2022 55th IEEE/ACM International Symposium on Microarchitecture (MICRO)*. IEEE, 1078–1091.
 - [29] Prakash Murali, Jonathan M Baker, Ali Javadi-Abhari, Frederic T Chong, and Margaret Martonosi. 2019. Noise-adaptive compiler mappings for noisy intermediate-scale quantum computers. In *Proceedings of the Twenty-Fourth International Conference on Architectural Support for Programming Languages and Operating Systems*. 1015–1029.
 - [30] Giacomo Nannicini, Lev S Bishop, Oktay Günlük, and Petar Jurcevic. 2022. Optimal qubit assignment and routing via integer programming. *ACM Transactions on Quantum Computing* 4, 1 (2022), 1–31.
 - [31] Siyuan Niu, Adrien Suau, Gabriel Staffelbach, and Aida Todri-Sanial. 2020. A Hardware-Aware Heuristic for the Qubit Mapping Problem in the NISQ Era. *IEEE Transactions on Quantum Engineering* 1 (2020), 1–14.
 - [32] Alexandru Paler, Austin G Fowler, and Robert Wille. 2017. Online scheduled execution of quantum circuits protected by surface codes. *arXiv preprint arXiv:1711.01385* (2017).
 - [33] Alexandru Paler, Alwin Zulehner, and Robert Wille. 2021. NISQ circuit compilation is the travelling salesman problem on a torus. *Quantum Science and Technology* 6, 2 (2021), 025016.
 - [34] Warren B Powell. 2009. What you should know about approximate dynamic programming. *Naval Research Logistics (NRL)* 56, 3 (2009), 239–249.
 - [35] John Preskill. 2018. Quantum Computing in the NISQ era and beyond. *Quantum* 2 (2018), 79.
 - [36] Krishanu Sankar, Artur Scherer, Satoshi Kako, Sam Reifenstein, Navid Ghadermarzy, Willem B. Krayenhoff, Yoshitaka Inui, Edwin Ng, Tatsuhiro Onodera, Pooya Ronagh, and Yoshihisa Yamamoto. 2021. Benchmark Study of Quantum Algorithms for Combinatorial Optimization: Unitary versus Dissipative. [arXiv:2105.03528 \[quant-ph\]](https://arxiv.org/abs/2105.03528)
 - [37] Eddie Schoute. 2020. *Circuit Transformations for Quantum Architectures*. Retrieved May 18, 2021 from <https://gitlab.umi.acs.umd.edu/amchilds/arct>
 - [38] Alireza Shafaei, Mehdi Saeedi, and Massoud Pedram. 2014. Qubit placement to minimize communication overhead in 2D quantum architectures. In *2014 19th Asia and South Pacific Design Automation Conference (ASP-DAC)*. IEEE, 495–500.
 - [39] Animesh Sinha, Utkarsh Azad, and Harjinder Singh. 2021. Qubit Routing using Graph Neural Network aided Monte Carlo Tree Search. *arXiv preprint arXiv:2104.01992* (2021).
 - [40] Marcos Yukio Siraichi, Vinícius Fernandes dos Santos, Sylvain Collange, and Fernando Magno Quintão Pereira. 2018. Qubit allocation. In *Proceedings of the 2018 International Symposium on Code Generation and Optimization*. 113–125.
 - [41] Seyon Sivarajah, Silas Dilkes, Alexander Cowtan, Will Simmons, Alec Edgington, and Ross Duncan. 2020. t|ket>: a retargetable compiler for NISQ devices. *Quantum Science and Technology* 6, 1 (2020), 014003.
 - [42] Bochen Tan and Jason Cong. 2021. Optimal qubit mapping with simultaneous gate absorption. *arXiv preprint arXiv:2109.06445* (2021).
 - [43] Arianne Meijer van de Griend and Sarah Meng Li. 2022. Dynamic qubit allocation and routing for constrained topologies by CNOT circuit re-synthesis. *arXiv preprint*

- arXiv:2205.00724* (2022).
- [44] LMK Vandersypen, H Bluhm, JS Clarke, AS Dzurak, R Ishihara, A Morello, DJ Reilly, LR Schreiber, and M Veldhorst. 2017. Interfacing spin qubits in quantum dots and donors—hot, dense, and coherent. *npj Quantum Information* 3, 1 (2017), 1–10.
 - [45] Davide Venturelli, Minh Do, Bryan O’Gorman, Jeremy Frank, Eleanor Rieffel, Kyle EC Booth, Thanh Nguyen, Parvathi Narayan, and Sasha Nanda. 2019. Quantum circuit compilation: An emerging application for automated reasoning. In *Proc. Schedul. Plan. Appl. Workshop*.
 - [46] Friedrich Wagner, Andreas Bärman, Frauke Liers, and Markus Weissenböck. 2022. Improving Quantum Computation by Optimized Qubit Routing. *arXiv preprint arXiv:2206.01294* (2022).
 - [47] Mathias Weiden, Justin Kalloor, John Kubiawicz, Ed Younis, and Costin Iancu. 2022. Wide Quantum Circuit Optimization with Topology Aware Synthesis. *arXiv preprint arXiv:2206.13645* (2022).
 - [48] Robert Wille, Aaron Lye, and Rolf Drechsler. 2014. Optimal SWAP gate insertion for nearest neighbor quantum circuits. In *2014 19th Asia and South Pacific Design Automation Conference (ASP-DAC)*. IEEE, 489–494.
 - [49] Xin-Chuan Wu, Marc Grau Davis, Frederic T Chong, and Costin Iancu. 2020. QGo: Scalable quantum circuit optimization using automated synthesis. *arXiv preprint arXiv:2012.09835* (2020).
 - [50] Amanda Xu, Abtin Molavi, Lauren Pick, Swamit Tannu, and Aws Albarghouthi. 2022. Synthesizing Quantum-Circuit Optimizers. *arXiv preprint arXiv:2211.09691* (2022).
 - [51] Xiangzhen Zhou, Yuan Feng, and Sanjiang Li. 2020. A monte carlo tree search framework for quantum circuit transformation. In *Proceedings of the 39th International Conference on Computer-Aided Design*. 1–7.
 - [52] Alwin Zulehner, Alexandru Paler, and Robert Wille. 2018. An efficient methodology for mapping quantum circuits to the IBM QX architectures. *IEEE Transactions on Computer-Aided Design of Integrated Circuits and Systems* 38, 7 (2018), 1226–1236.
 - [53] Alwin Zulehner, Alexandru Paler, and Robert Wille. 2019. *Mapping of OPENQASM programs to IBM QX satisfying the architectural constraints*. Retrieved March 08, 2021 from http://github.com/iic-jku/ibm_qx_mapping/tree/master/examples

APPENDIX

Appendix A: Hyperparameter Selection

We have introduced several hyperparameters in the placement and routing algorithm, and have studied their effects on the performance of our transpiler. The hyperparameters we have used are as follows:

- Discount factor δ : This discount factor is used in the definitions of the edge scores Ω and placement scores Σ . The closer the discount factor is to 1, the more significant is the contribution of future gates in calculating the scores.
- Decision horizon λ : This hyperparameter determines the number of gates that are to be included in the calculations of the edge scores Ω and the placement scores Σ . A higher value of λ indicates that a greater number of gates will be included in the score calculations.
- Lookahead depth D : This hyperparameter determines how many future actions (i.e., SWAP gate insertions) the tie-breaking subroutine looks ahead from, within the decision horizon.

To understand how the hyperparameters affect SWAP count, we generate six families of circuits: adder, amplitude estimation, Grover’s search, phase estimation, quantum Fourier transform (QFT), and random. All circuits follow Qiskit’s implementation [15].

We first vary the value of δ and fix the decision horizon at $\lambda = 100$ and lookahead depth at $D = 9$. From Fig. 7, higher values of δ in general result in lower SWAP counts. We refer to the δ values of 0.7, 0.9, and 1 as *large* δ values. For adder circuits with 4, 8, 12, and 16 qubits, we attain the lowest SWAP counts using large δ , while for the adder circuit with 20 qubits, a value of $\delta = 0.1$ results in the lowest SWAP count, followed closely by $\delta = 0.9$. In other words, using a large δ value results in the lowest SWAP count in 80% of the test cases for adder circuits. For the amplitude estimation, Grover’s search, phase estimation, QFT, and random circuits, using a large δ value, we attain a lowest SWAP count of 81.25%, 63.63%, 80%, 70.59%, and 55.56% respectively.

Figure 8 shows that the value of λ does not affect the SWAP count in the case of the adder, amplitude estimation, QFT, and random circuits. As for the Grover’s search and phase estimation circuits, we observe that a higher value of λ usually results in a lower SWAP count, except for the Grover’s search circuit with 14 qubits, and the phase estimation circuits with 7, 8, 10, 14, and 15 qubits. However, even for circuits that do not result in the lowest SWAP count using high values of λ , we observe that the difference in SWAP count is not significant. Therefore, we conclude that having a higher value of λ is in general beneficial.

Having understood that λ does not on its own affect SWAP counts significantly, we design another experiment where we fix the ratio between λ and D . We set λ to a certain percentage of the number of gates in the circuits and fix the value of D to be half that of λ . The result is shown in Fig. 9. We observe that for the amplitude estimation, Grover’s search, and phase estimation circuits, higher values of λ and D result in the majority of cases where the SWAP count is lowest, while the results for the adder, QFT, and random circuits are inconsistent. It is worth noting that the results for the amplitude estimation and Grover’s search circuits overlap to a great extent, indicating that the circuits are not sensitive to the value of either λ or D ; in other words, once the values of λ and D exceed a certain threshold, the SWAP count will not decrease further even if larger values of λ and D are used. We suspect that this is due to the structure of the amplitude estimation and Grover’s search circuits, where a lot of two-qubit gates are situated between single-qubit gates. When the two-qubit gates do not commute with the single-qubit gates, they need to be executed in sequential order. Thus, the effects of λ and D become negligible.

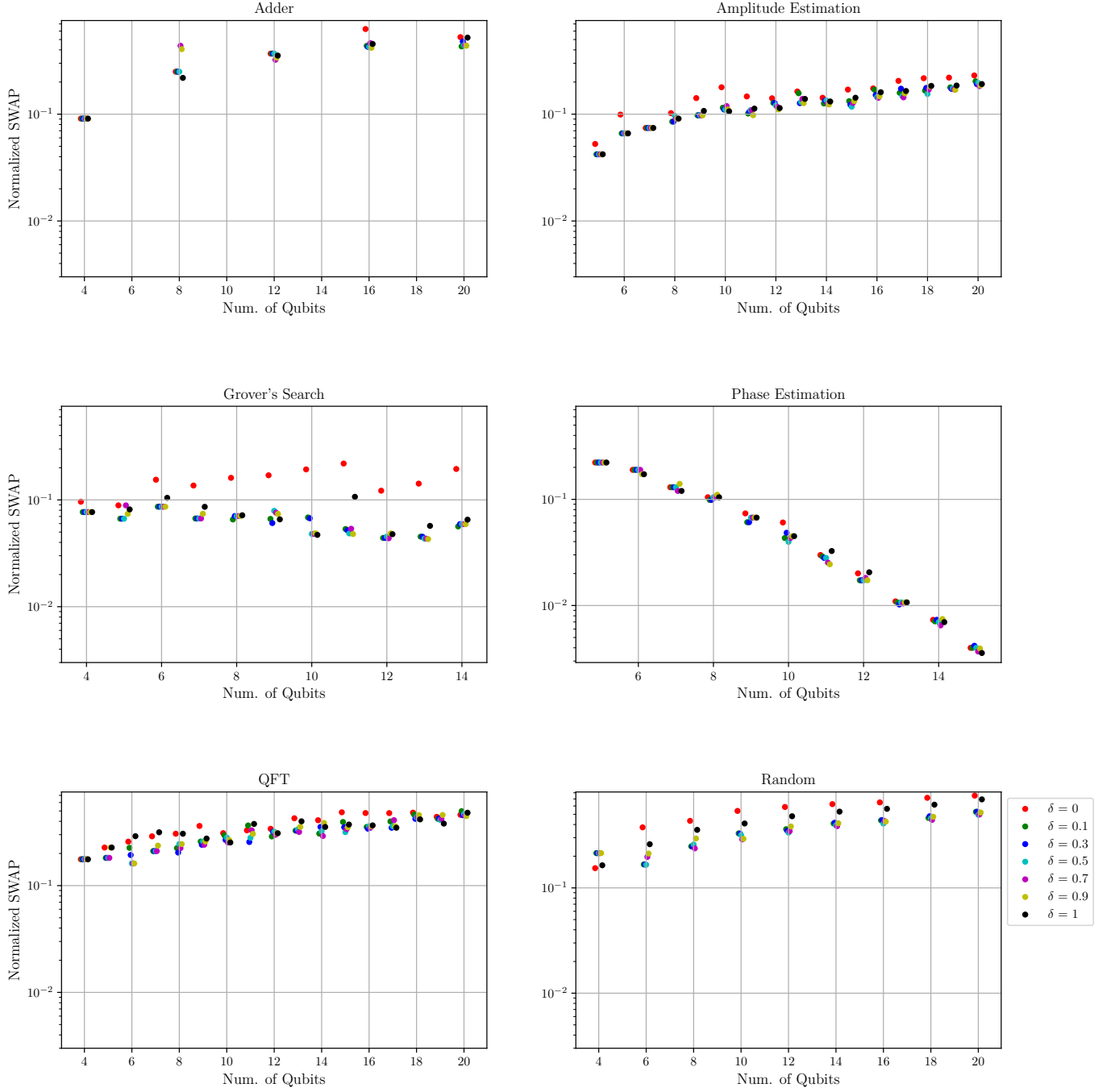


FIG. 7. Varying the discount factor δ with the depth $D = 9$ and the decision horizon $\lambda = 100$. The SWAP count is normalized by the number of gates in the circuits. We offset the points representing the normalized SWAP values in the x direction for visual clarity.

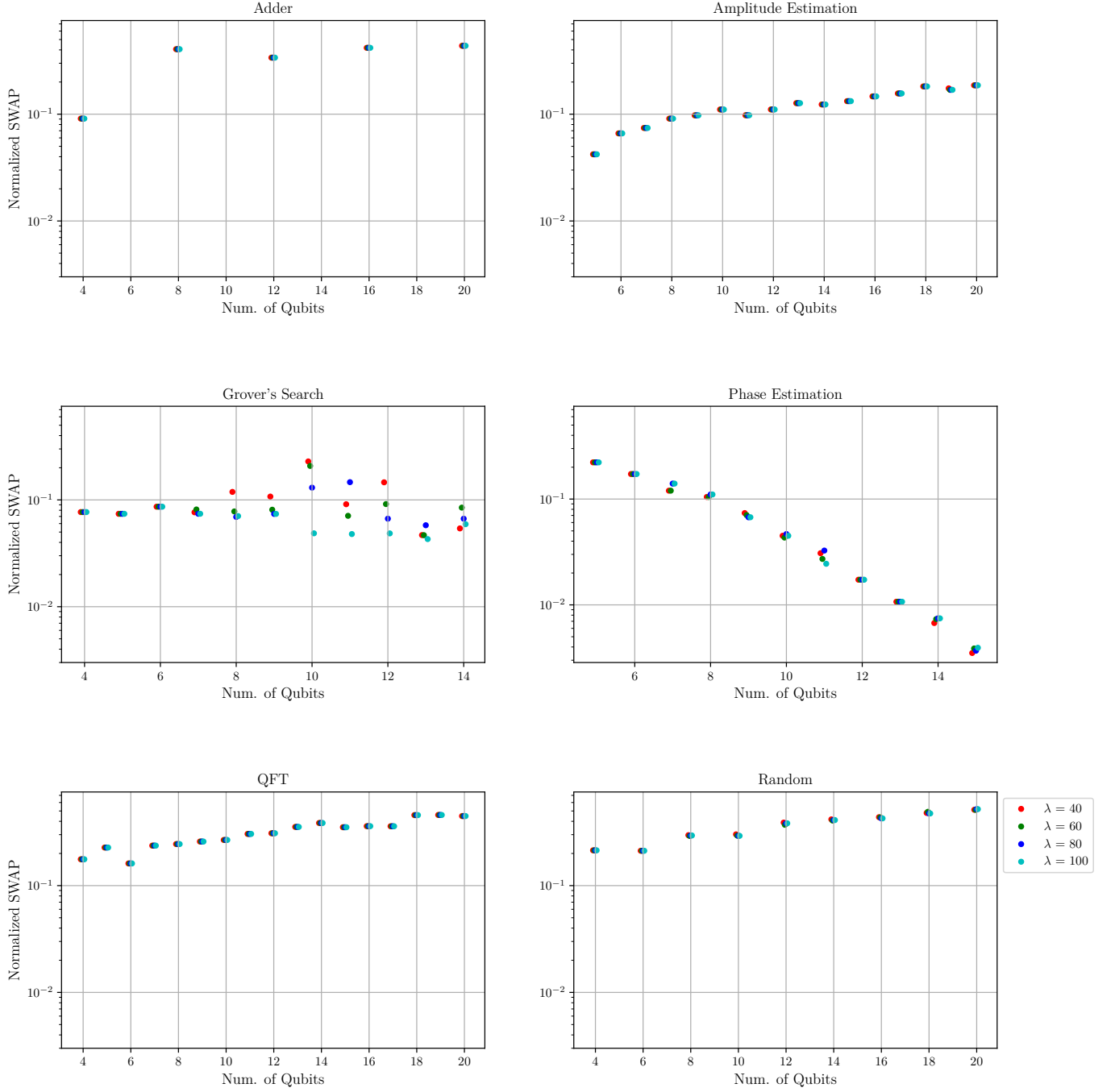


FIG. 8. Varying the decision horizon λ with the depth $D = 9$ and the discount factor $\delta = 0.9$. The SWAP count is normalized by the number of gates in the circuits. We offset the points representing the normalized SWAP values in the x direction for visual clarity.

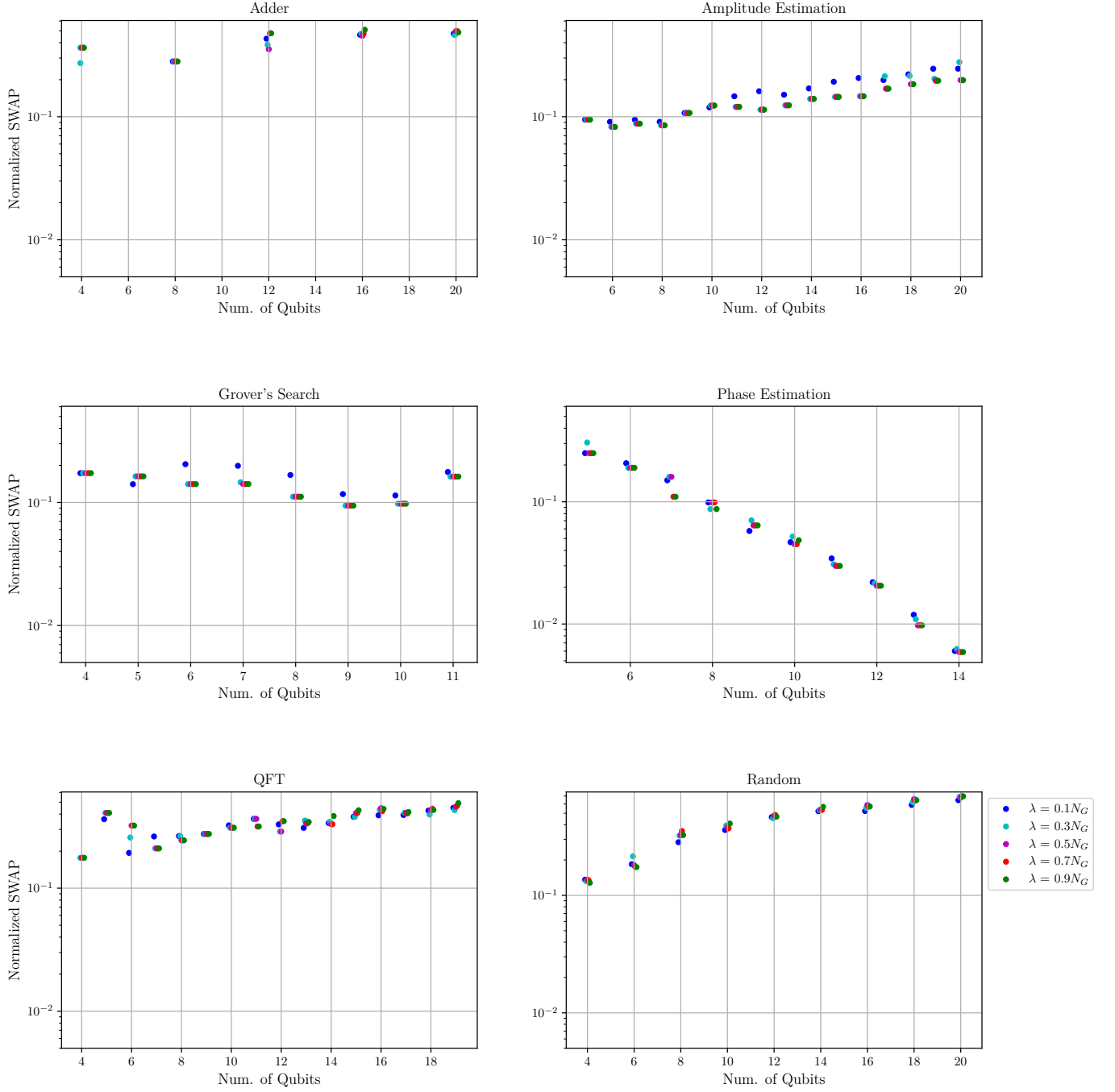


FIG. 9. Varying the decision horizon λ with the discount factor $\delta = 0.9$ and the lookahead depth $D = 0.5\lambda$. The total number of gates in a test circuit is denoted by N_G . The SWAP count is normalized by the number of gates in the circuits. We offset the points representing the normalized SWAP values in the x direction for visual clarity.

Appendix B: Detailed Benchmarking Results

Table IV shows the detailed benchmarking results for **tket**, **SABRE**, and **Nuwa** transpiling input circuits onto the coupling graphs of two target architectures: the IBM Q20 Tokyo chip and a 4 x 5 grid. In order to study

the routing algorithms in isolation, we use a naïve fixed placement (i.e., matching the vertex and qubit numbers) across all experiments. We provide a visualization of these results in Fig. 10. The benchmarking circuit instances may be found in [53].

Input Circuit Name	No. of Qubits	No. of Gates	IBM Q20 Tokyo Graph			4 × 5 Grid		
			tket	SABRE	Nuwa	tket	SABRE	Nuwa
xor5_254	6	7	1*	5	3	2*	5	3
graycode6_47	6	5	1*	2	6	2*	3	5
ex1_226	6	7	1*	2	3	2*	4	3
4gt11_84	4	18	3	7	2*	3	7	2*
4mod5-v0_20	5	20	3*	4	3*	3*	4	5
ex-1_166	3	19	3*	6	3*	3*	6	3*
4mod5-v1_22	5	21	4	7	1*	4	7	3*
mod5d1_63	5	22	1*	12	4	5	13	4*
ham3_102	3	20	3	6	2*	3	6	2*
4gt11_83	5	23	4*	10	4*	4*	7	4*
4gt11_82	5	27	5*	11	5*	6	10	4*
rd32-v0_66	4	34	6	14	1*	6*	14	6*
alu-v0_27	5	36	3*	13	4	7	12	6*
4mod5-v1_24	5	36	8	12	6*	8	14	7*
4mod5-v0_19	5	35	3*	16	5	7*	16	10
mod5mils_65	5	35	3*	17	5	6*	17	10
rd32-v1_68	4	36	6	14	1*	6*	14	6*
alu-v1_28	5	37	4*	12	5	8	12	7*
alu-v2_33	5	37	3*	10	3*	6*	10	8
alu-v4_37	5	37	3*	14	4	7	17	6*
alu-v3_35	5	37	3*	10	4	7	12	6*
3_17_13	3	36	6	13	1*	6	11	5*
alu-v1_29	5	37	4*	10	4*	8	10	6*
millar_11	3	50	9	19	0*	9*	19	9*
alu-v3_34	5	52	6	20	3*	10*	25	12
decod24-v2_43	4	52	9	20	2*	9	20	8*
decod24-v0_38	4	51	6*	17	7	9	18	8*
mod5d2_64	5	53	6*	26	8	11*	25	12
4gt13_92	5	66	9*	21	9*	12	29	11*
4gt13-v1_93	5	68	6*	24	7	12	27	9*
4mod5-v0_18	5	69	4*	31	9	12*	31	14
decod24-bdd_294	6	73	9*	20	13	13*	23	14
one-two-...v2_100	5	69	7	22	4*	14	23	11*
one-two-...v3_101	5	70	7*	21	8	13*	21	14
4mod5-v1_23	5	69	4*	35	9	14	33	12*
4mod5-bdd_287	7	70	7*	13	8	14*	24	15
rd32_270	5	84	6*	34	11	16*	34	16*
4gt5_75	5	83	9*	34	11	16	34	12*
alu-bdd_288	7	84	15	11	9*	16*	17	17
alu-v0_26	5	84	10	34	9*	16	34	14*
decod24-v1_41	5	85	14	26	6*	17	34	16*
rd53_138	8	132	11*	23	12	25*	38	31
4gt5_76	5	91	14	28	12*	17*	40	17*
4gt13_91	5	103	13	39	12*	19*	38	21
cnt3-5_179	16	175	31	26	24*	52	38*	40
qft_10	10	200	16*	57	22	24*	60	25
4gt13_90	5	107	15	43	12*	20*	40	21
alu-v4_36	5	115	13*	41	13*	20	43	18*
mini_alu_305	10	173	27	41	22*	39	46	34*
ising_model_10	10	480	9	66	4*	15	30	11*
ising_model_16	16	786	11*	76	17	46	75	16*
ising_model_13	13	633	9*	43	15	26*	82	27
4gt5_77	5	131	18	51	13*	22*	51	24
sys6-v0_111	10	215	22	44	21*	50	54	45*

one-two-...v1_99	5	132	15	59	11*	27*	58	28
one-two-...v0_98	5	146	16	47	11*	25	64	21*
decod24-v3_45	5	150	19	42	15*	25*	57	27
4gt10-v1_81	5	148	24	40	11*	27*	62	29
aj-e11_165	5	151	27	45	14*	28	55	26*
4mod7-v0_94	5	162	17*	45	19	30	63	27*
alu-v2_32	5	163	23	57	14*	29*	64	30
rd73_140	10	230	19*	57	24	51	57	49*
4mod7-v1_96	5	164	24	45	10*	31	64	28*
4gt4-v0_80	6	179	11*	36	17	34	42	33*
mod10_176	5	178	26	58	18*	33	75	28*
0410184_169	14	211	33*	50	36	58	55*	56
qft_16	16	512	55	137	40*	79	142	55*
4gt12-v0_88	6	194	31	41	22*	45	46	33*
rd84_142	15	343	37	57	36*	74	62*	72
rd53_311	13	275	51	56	26*	64	94	62*
4_49_16	5	217	33	76	21*	44	87	36*
sym9_146	12	328	30*	59	31	70	100	60*
4gt12-v1_89	6	228	26	76	14*	41	64	40*
4gt12-v0_87	6	247	21*	31	28	45	73	41*
4gt4-v0_79	6	231	15*	35	30	43	67	39*
hwb4_49	5	233	22*	94	24	41	94	37*
sym6_316	14	270	43	62	41*	59*	79	67
4gt12-v0_86	6	251	22*	31	30	46	76	41*
4gt4-v0_72	6	258	28	45	27*	53	99	44*
4gt4-v0_78	6	235	17*	36	32	44	68	40*
mod10_171	5	244	33	81	25*	44	89	43*
4gt4-v1_74	6	273	37	61	27*	64	87	45*
rd53_135	7	296	23*	76	23*	59	88	56*
mini-alu_167	5	288	38	96	35*	53	115	49*
one-two-...v0_97	5	290	41	122	36*	56	121	48*
ham7_104	7	320	43	61	17*	62	82	58*
decod24-enable...	6	338	35	75	20*	62	124	58*
mod8-10_178	6	342	29	71	23*	78	105	59*
cnt3-5_180	16	485	83	127	32*	107	130	104*
ex3_229	6	403	52	81	39*	92	115	64*
4gt4-v0_73	6	395	43	89	25*	79	145	72*
mod8-10_177	6	440	44	97	35*	86	115	72*
C17_204	7	467	70	134	25*	89*	167	91
alu-v2_31	5	451	42*	141	42*	90	196	76*
rd53_131	7	469	46	94	33*	94	147	88*
alu-v2_30	6	504	59	104	39*	96	181	93*
mod5adder_127	6	555	83	102	49*	121	184	96*
rd53_133	7	580	108	195	26*	121	156	98*
cm82a_208	8	650	69	160	29*	120*	180	125
majority_239	7	612	75	176	42*	121	192	105*
ex2_227	7	631	89	194	31*	119	220	101*
sf_276	6	778	76	127	54*	147	262	127*
sf_274	6	781	84	209	76*	172	201	137*
con1_216	9	954	178	227	40*	193	307	170*
wim_266	11	986	125	224	78*	227	307	184*
rd53_130	7	1043	106	219	72*	239	290	184*
f2_232	8	1206	194	343	73*	252	343	217*
cm152a_212	12	1221	202	260	79*	273	354	213*
rd53_251	8	1291	172	205	100*	278	406	233*
hwb5_53	6	1336	153	328	110*	254	397	245*
cm42a_207	14	1776	236	412	92*	374	489	305*
pm1_249	14	1776	236	285	92*	374	558	305*
dc1_220	11	1914	278	309	92*	396	610	338*
squar5_261	13	1993	339	392	128*	445	546	355*
z4_268	11	3073	369	668	216*	750	874	537*
sqrt8_260	12	3009	476	552	252*	725	881	575*
radd_250	13	3213	468	635	205*	708	939	608*
adr4_197	13	3439	495	641	224*	719	936	638*

sym6_145	7	3888	332	1043	214*	759	1107	680*
misex1_241	15	4813	589	938	253*	993	1407	909*
rd73_252	10	5321	690	1043	389*	1118	1664	976*
cycle10_2_110	12	6050	910	1276	423*	1354	1624	1089*
hwb6_56	7	6723	956	1438	409*	1321	1998	1184*
square_root_7	15	7630	1001	1118	504*	1640	2156	1301*
ham15_107	15	8763	1163	1636	589*	1909	2408	1615*
dc2_222	15	9462	1200	2086	714*	2110	2599	1752*
sqn_258	10	10223	1100	2416	709*	2352	3212	1870*
inc_237	16	10619	1232	1904	600*	2351	2964	1888*
cm85a_209	14	11414	1720	2173	699*	2553	3315	2076*
rd84_253	12	13658	1914	3265	1188*	3130	4132	2537*
co14_215	15	17936	2583	3922	1054*	4364	5220	3577*
root_255	13	17159	2547	3535	1328*	3824	4915	3152*
mlp4_245	16	18852	2168	4073	1463*	4223	5396	3572*
urf2_277	8	20112	3321	4434	2191*	5543	6469	4091*
sym9_148	10	21504	2852	4596	886*	5473	6060	3706*
life_238	11	22445	3266	4570	1551*	5287	6272	4157*
hwb7_59	8	24379	2956	5076	1854*	4768	6791	4196*
max46_240	10	27126	3697	5941	1984*	5894	8226	4796*
clip_206	14	33827	4505	7147	2063*	7958	9833	6319*
9symml_195	11	34881	5232	7504	2537*	8268	9545	6441*
sym9_193	11	34881	5232	6995	2537*	8268	9803	6441*
sao2_257	14	38577	4312	7966	2083*	8938	10798	7310*
dist_223	13	38046	4707	7939	2182*	8582	10704	7075*
urf5_280	9	49829	6520	11229	4277*	11720	16416	9596*
urf1_278	9	54766	10646	12291	5187*	15126	18407	10727*
sym10_262	12	64283	9810	13513	4872*	14673	17856	12177*
hwb8_113	9	69380	11874	13697	4904*	15758	21123	12062*
urf2_152	8	80480	7748	15376	6612*	15923	23620	13928*
urf3_279	10	125362	19498	29663	11219*	31126	41320	25021*
plus63mod...163	13	128744	20470	27511	9618*	30692	37207	24375*
urf5_158	9	164416	22682	32133	13220*	34169	49734	28583*
urf6_160	15	171840	22359	35154	16218*	38318	48154	33050*
urf1_149	9	184864	21828	37104	16367*	38558	56099	31928*
plus63mod...164	14	187112	24956	38682	14438*	44366	54477	35014*
hwb9_119	10	207775	27687	39659	14569*	47846	62845	37163*
urf3_155	10	423488	51978	84436	35888*	89626	126737	76050*
ground_...10	13	390180	15612	5586*	8947	22169	13030*	14378
urf4_187	11	512064	86174	87487	33856*	118263	139987	90583*
Number of Lowest SWAP Counts			44	1	123*	34	4	127*

TABLE IV: SWAP counts for **tket**, SABRE, and Nuwa. The lowest SWAP count achieved for each circuit is shown in bold text and with an astrisk. Columns 4 to 6 show the results for the IBM Q20 Tokyo coupling graph represented in Fig. 1(b) and columns 7 to 9 show tests performed on a 4×5 target architecture.

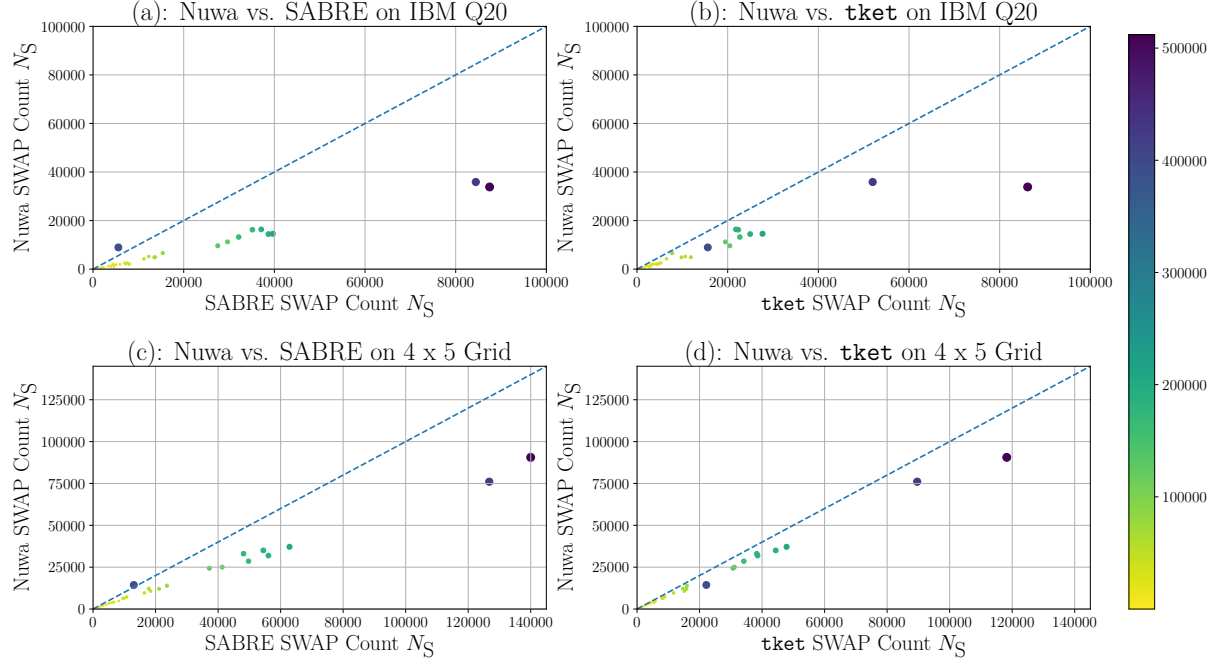


FIG. 10. A plot corresponding to Table IV. (a) SWAP counts of Nuwa vs. SABRE on the IBM Q20. (b) SWAP counts of Nuwa vs. `tket` on the IBM Q20. (c) SWAP counts of Nuwa vs. SABRE on a 4 x 5 grid. (d) SWAP counts of Nuwa vs. `tket` on a 4 x 5 grid. The colours and sizes of the dots correspond to the number of gates in the circuit.